Rev.Adv.Mater.Sci. 10 (2005) 39-44

FABRICATION AND MICROSTRUCTURAL CHARACTERIZATION OF NANO-CRYSTALLINE ZrO_2-BASED COMPOSITE

Koji Morita, Keijiro Hiraga, Byung-Nam Kim, Hidehiro Yoshida and Yoshio Sakka

National Institute for Materials Science, 1-2-1 Sengen, Tsukuba, Ibaraki 305-0047, Japan

Received: April 28,2005

Abstract. Nanocrystalline ZrO_2-spinel powders consisting of nano-particles of ≤10 nm can successfully be synthesized using high-energy ball-milling process. Using spark-plasma-sintering technique, the nanocrystalline powders can be consolidated into dense nanocrystalline composite with an average grain size of <100 nm. The mechanical properties of ZrO_2-spinel composite can significantly be improved by the nano-crystalization. Flexural strength σ_f was heightened by a factor of 2.0-2.5: the maximum σ_f of the nanocrystalline composite reached ≈2.4 GPa. Flow stress of the nanocrystalline composite can be lowered by about 50% than that of submicrometer-sized composite.

1. INTRODUCTION

Tetragonal zirconia (t-ZrO_2) ceramics have excellent mechanical properties [1]. Use for engineering applications of ZrO_2, however, has been limited because of its lower formability. Although superplasticity attained in several ZrO_2-based ceramics [2], the available strain rates are too lower for near-net-shaping applications. Recently, we can improve the superplasticity of ZrO_2 ceramics by the dispersion of fine $MgAl_2O_4$ spinel particles: high-strain-rate superplasticity (HSRS) that is defined as an ability of a material to show a tensile elongation of >200% at strain rates of $\geq 10^{-2}$ s^{-1} was attained in the ZrO_2-spinel composite at ≥1673K [3,4]. For the use for near-net-shaping applications, further improvement of superplastic properties is required: low forming temperature and high available strain rate. In addition, mechanical properties are also important for engineering applications.

To attain these requirements in ceramic materials, nano-crystallization seems to be one of the promising ways. For superplasticity, grain size is a critical factor to improve forming temperature and available strain rate [2]. Furthermore, recent studies [5-10] have shown that, as compared with submicrometer-sized ceramics, the nanocrystalline ceramic materials can exhibit excellent mechanical properties as grain size is reduced to less than 100 nm.

The present study was therefore performed to synthesize the nanocrystalline ZrO_2-30vol.% $MgAl_2O_4$ spinel composite. In order to synthesize the nanocrystalline composite, we employed high-energy ball-milling (HEBM) and spark-plasma-sintering (SPS) techniques.

Corresponding author: Koji Morita, e-mail: MORITA.Koji@nims.go.jp

2. EXPERIMENTAL PROCEDURES

2.1. Material preparation

The powders used were a high-purity 3mol.%-Y_2O_3-stabilized tetragonal ZrO_2 powder (>99.97%, Tosoh Co., Ltd.,) and a high-purity $MgAl_2O_4$ spinel powder (>99.97, Taimei Chemical Co. Ltd.). The average particle sizes were ≈270 nm for ZrO_2 and ≈360 nm for spinel. Tetragonal ZrO_2 powder mixed with 30 vol.% spinel powder was milled with a planetary ball-milling machine for 0-400 h in ethanol using ZrO_2 ball and pot.

The ball-milled powders were consolidated with a SPS machine (Sumitomo Coal Mining Co., Japan). The powders were placed into a graphite die and rapidly heated up to 1573K at a heating rate of about 100 °C/min under vacuum, and then held at the temperature for 5 min. The temperature was controlled by monitoring the surface temperature of the graphite die with an optical pyrometer. In this procedure, we have prepared circular disks of 30 mm in diameter and 2 mm in thickness. The relative density of the SPSed specimens was measured by the Archimedes method, where the theoretical density was defined as $5.322 \cdot 10^3$ kg/m^3 according to the rule of mixture.

2.2. Microstructural characterization

The phases of the ball-milled powders and the SPSed specimens were determined by X-ray diffraction (XRD) using Cu$K\alpha$ radiation operating at 40 kV and 300 mA. The microstructural observations were conducted by transmission electron microscopy (TEM) and scanning electron microscopy (SEM). For TEM observation of HEBM processed powders, a small amount of powders dispersed in ethanol was dropped on Cu micro-grid equipped with carbon substrate. For bulk specimens, thin sheets with a thickness of about 500 μm were with a low-speed diamond cutter, mechanically polished to about 100 μm in thickness and further thinned with an Ar ion-milling machine. For SEM observation, the surface of the bulk specimens were mechanically polished and thermally etched at 1473K for 10 min. The average grain size, *d*, was determined as 1.56 times of the average intercept lengths of grains [11].

2.3. Mechanical properties

Flexural strength σ_f was measured by three-point-bending test at room temperature. The SPSed circular disks were cut into rectangular bars of 2.4 mm width and 1.5 mm thickness. The measurements were performed at a 16 mm span and a cross-head displacement rate of 0.5 mm/min. For tensile tests, dog-bone-shaped flat tensile specimens were machined with gauge portions of ^{t}2-^{w}3-^{l}10 mm. Constant displacement-rate tensile tests were conducted at 1573-1723K and at initial strain rates of $\dot{\varepsilon}_0 \approx 3.3 \cdot 10^{-4} - 0.7$ s^{-1} under vacuum.

3. RESULTS AND DISCUSSION

3.1. Ball mill processed powder

Fig. 1a shows XRD profiles of HEBM processed ZrO_2-30 vol.% spinel powders. For the as-mixed powder, all the sharp peaks can be indexed from tetragonal (t-) ZrO_2, monoclinic (m-) ZrO_2 and spinel phases but no cubic (c-) ZrO_2 phase was detected. For the HEBM processed powders, the peaks become broad as milling process proceeds.

It can be seen from the inspection of the XRD profile that a gradual phase transformation from t-ZrO_2 to m-ZrO_2 occurs through HEBM process. The stability of the two phases has been interpreted mainly from surface energy and secondary from internal strains and impurities [12]. Since the surface energy of the t-phase is lower than that of the m-phase, the t-phase becomes stable rather than m-phase with a decrease in particle size. The present result appears to be inconsistent with this stability. From the broad XRD profile, it is clear that the large strain was induced into the crystals by high impact energy of the ZrO_2 ball. Although the difference in the transformation behavior is unclear at the present time, the large strain is likely to be responsible for the m-ZrO_2 transformation.

A change in microstructure was characterized by high-resolution TEM (HRTEM) and EDS. For the as-mixed powder, the particles had sharp shapes and the corresponding selected area diffraction (SAD) pattern showed a sharp ring pattern. HRTEM observation showed that the starting powders consisted of single or single-like crystals. After the HEBM process, the contrasts of the powders and the corresponding SAD pattern become diffuse as milling process proceeds. (Figs. 1b and 1c). HRTEM observation revealed that, after 250 h ball-milling, the powder is composed of nanocrystalline particles of about 10 nm or less. After 400 h ball-milling, an amorphous-like phase is formed among the nanocrystalline particles.

The change in the microstructure corresponds to the result of XRD in Fig. 1a. For the HEBM processed powders, since much lattice distortion and

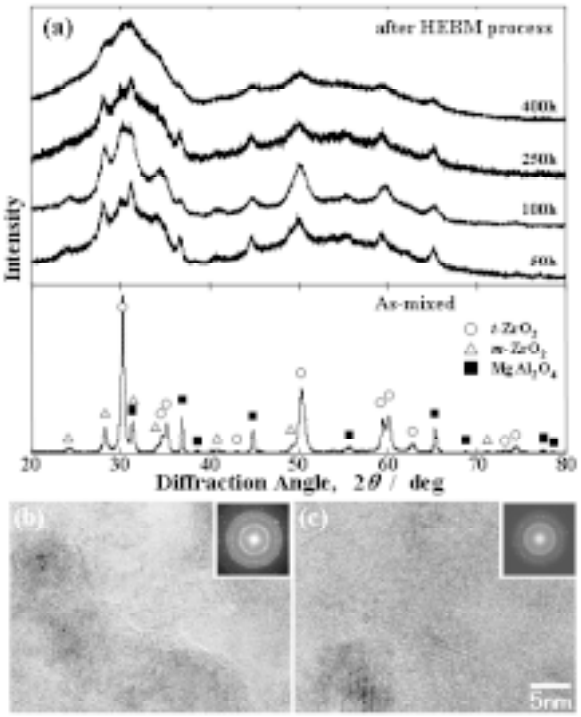

Fig. 1. (a) XRD profiles for ZrO_2-30vol.% spinel powders after ball-milling for 0-400 h and high-resolution TEM images and corresponding SAD patterns of the ball-milled powders for (b) 250 h and (c) 400 h.

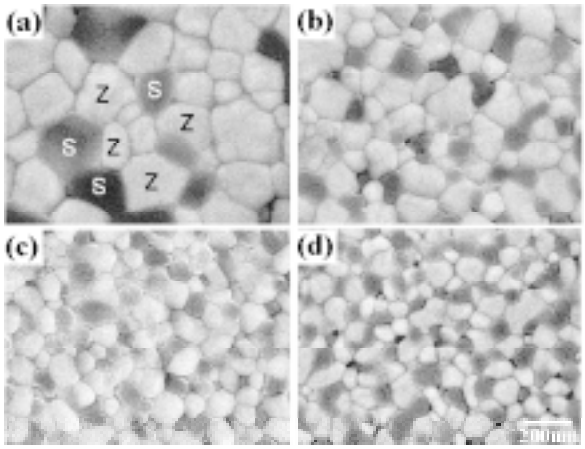

Fig. 2 Typical SEM images of ZrO_2-30 vol.% spinel composites; (a) pressureless-sintered in air at 1673K for 2 h and SPSed at 1573K for 5 min after ball-milling for (b) 50 h, (c) 250 h and (d) 400 h. The bright and dark contrasts correspond to ZrO_2 (Z) and spinel (S) phases, respectively.

many twins were observed in the nanocrystalline particles, the nano-crystallization and residual strain induced by impact energy of the ZrO_2 ball is likely to be responsible for the broadening of XRD profile. For 400 h HEBM processed powder, amorphization would result in the limited weak peak in the broad XRD patterns.

EDS analysis confirmed that the amorphous-like phase consists mainly of the mixture of zirconium, aluminum and magnesium, and no impurity was detected. Since such an amorphous-like phase was observed to form in the nanocrystalline powders as HEBM process proceeds, the contamination during HEBM process is unlikely responsible for the amorphization. According to the study by Hankey *et al*. [13], although large residual strain and reduced crystalline size are one of the important factors affecting solid state reactivity, the reactivity was enhanced mainly by high pressure shock. Therefore, the amorphization must occur through the solid state reaction induced by high impact energy induced during HEBM process.

3.2. Microstructure of SPSed materials

Fig. 2 shows SEM images of ZrO_2-30vol.% spinel composite SPSed at 1537K for 5 min. For comparison, the microstructure of ZrO_2-spinel composite pressureless-sintered in air at 1673K for 2 h is also shown in Fig. 2a. For the pressureless-sintering, although we obtained dense sintered bodies with $\rho > 98$ %, the average grain sizes d exceeded 300 nm. For the HEBM and SPS processed composites, dense nanocrystalline composite of $\rho > 98\%$ can be obtained as shown in Figs. 2b-2d.

The properties of nanocrystalline ZrO_2-spinel composite are listed in Table 1. Using HEBM process, the grain size steeply decreases smaller than 150 nm at 100 h milling. After 400 h milling, dense nanocrystalline ZrO_2-spinel composite of $d \approx 96$ nm can successfully be synthesized. In general, fine powders tend to agglomerate, resulting in residual flaws. It is noted, however, that the spinel particles disperse homogenously among the ZrO_2 matrix and no detectable agglomeration was found as shown in Fig. 2d. After the SPS process, all the detected peaks can be indexed from the t-ZrO_2 and spinel phases.

3.3. Flexural strength

The flexural strength, σ_f, of the ZrO_2-spinel composite was examined as a function of grain size. σ_f of

Table 1. The present data of ball-milling time *t*, grain size *d* and density ρ, for ZrO_2-30 vol.% spinel composites ball-milled for 0-400 h.

specimen	ball-milling time, *t*(h)	density, ρ (%)	avarege grain size *d* (nm)
ZrO_2-30 vol.% spinel	0	98.0	300
	50	98.3	174
	100	99.3	127
	250	98.4	102
	450	98.5	96

the composite tends to increase with decreasing grain size as shown in Fig. 3a. For the submicrometer-sized composite with $d \approx 300$ nm, an average σ_f is about 0.9 GPa, which is lower than the σ_f-value in monolithic t-ZrO_2 [14]. For the nanocrystalline composite with $d \approx 96$ nm, on the other hand, σ_f reached high values as high as 1.9 GPa. The maximum strength of $\sigma_f \approx 2.2$ GPa reached almost the same level of $\sigma_f \approx 2.4$ GPa reported in ZrO_2-Al_2O_3 composite [15,16], which is classed to the highest σ_f in oxide ceramic materials. The refinement of grain size smaller than 100 nm can improve σ_f of the ZrO_2-spinel composite by a factor of 2.0-2.5.

According to earlier studies [1,17,18], the flexural strength σ_f of ZrO_2 ceramics has often been related to two different factors using the following equation

$$\sigma_f \propto K_{IC}\, a^{-1/2}, \quad (1)$$

where K_{IC} is the fracture toughness and *a* is the radius of critical flaw. For ZrO_2 ceramics, the K_{IC} value has often been related to stress-induced t → m phase transformation toughening, where the martensitic transformation strains can dissipate a portion of the energy of fracture [1,19]. As expected from Eq. (1), σ_f will increase with toughness K_{IC} for a constant *a*-value. XRD analysis showed, however, that a small amount of t → m phase transformation was detected on the fracture surfaces in the submicrometer-sized composite, but not for the high strength nanocrystalline composite. For the present composite, therefore, the strengthening would not contribute mainly to K_{IC} due to the t → m phase transformation.

According to the relation between σ_f and *a* in Eq. (1), a reduction of residual flaw size is effective

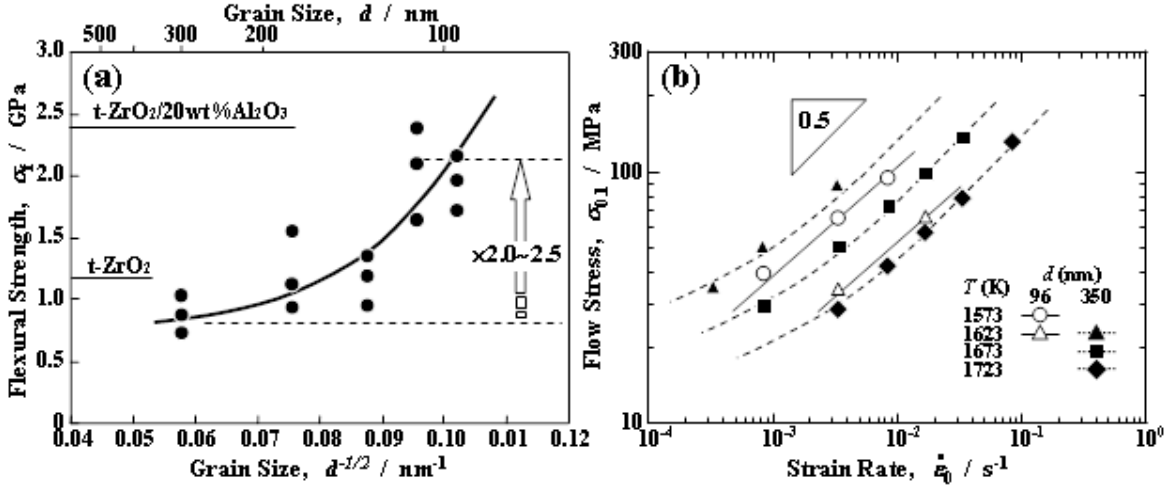

Fig. 3. Mechanical properties of nanocrystalline ZrO_2-30vol.% spinel composite; (a) flexural strength vs. milling time and (b) tensile flow stress vs. strain rate plots.

in increasing σ_f. From SEM examination of fracture origin, Tsukuma *et al.* [16] and Lange [20] have actually showed that σ_f is sensitive to residual flaw size and inhomogenous microstructures. In general, the flaw size is proportional to the grain size in dense materials. Thus, the attained dense and homogeneous nano-structure smaller than 100 nm would act as a possible factor for increasing σ_f of the present ZrO_2-spinel composite.

3.4. Tensile properties

Fig. 3b shows flow stress (σ)-strain rate ($\dot{\varepsilon}_0$) relationship of nanocrystalline ZrO_2-spinel composite. For comparison, the data of submicrometer-sized composite with d = 350 nm is also shown by closed symbols [4]. It is apparent from the inspection of Fig. 3b that a decrease in grain size can improve the deformability. The nano-crystalization enhances strain rate of one order of magnitude and decreases deformable temperature of the order of 100K.

The flow mechanism has often been characterized by the strain rate sensitivity m defined by the following creep equation:

$$\dot{\varepsilon} = A\sigma^{1/m} d^{-p}, \quad (2)$$

where $\dot{\varepsilon}$ is the steady-state strain rate, d is the grain size, p is the grain size exponent and A is a constant. In the both materials, the m-value estimated from the slop in the σ-$\dot{\varepsilon}_0$ relationship takes almost the same value of 0.5. For fine-grained ceramics with $m \approx 0.5$, grain boundary sliding (GBS) process has generally been regarded as the most important high-temperature flow mechanism [2]. It is therefore reasonable to explain that the deformation of the nanocrystalline ZrO_2-spinel composite occurs primarily through GBS. The improvement of deformability would not result from the change in flow mechanism but from the decreases in grain size as expected from Eq. (2).

In general, tensile elongation tends to increase with decreasing flow stress. In the present composite, however, the elongation of nanocrystalline composite is lower than that of submicrometer-sized one though flow stress was lowered due to nano-crystalization. Although the limited elongation in nanocrystalline composite is unclear at the present time, the preexisted nano-sized flaw is likely to be responsible for the lower tensile elongation.

4. SUMMARY

In order to synthesize nanocrystalline zirconia-spinel composite, HEBM and SPS techniques were employed. The results obtained are as follows.

(1) Using the HEBM process, nanocrystalline ZrO_2-spinel powders with particle sizes of ≤10 nm can successfully be synthesized. After 400 h ball-milling, the powders consist of the mixture of nanocrystalline particles of the sizes smaller than 10 nm and an amorphous-like phase alloyed in an atomic level.

(2) Using SPS technique, the nanocrystalline ZrO_2-spinel powders can be consolidated into dense nanocrystalline composite with ρ > 98% and d < 100 nm.

(3) Nano-crystalization can strengthen the ZrO_2-spinel composite by a factor of 2.0-2.5. The maximum σ_f of the nanocrystalline composite reached ≈2.2 GPa. The high σ_f can be associated mainly with a decrease in flaw size due to nano-crystalization.

(4) Flow stress of the nanocrystalline composite can be lowered by 50% than that of submicrometer-sized composite.

ACKNOWLEDGEMENT

The authors are grateful to the Mitsubishi Foundation for supporting the present work.

REFERENCES

[1] D.J. Green, R.H.J. Hannink and M.V. Swain, In: *Transformation Toughening of Ceramics* (CRC press, 1989).

[2] T.G. Nieh, J. Wadsworth and O.D. Sherby, In: *Superplasticity in Metals and Ceramics* (Cambridge University Press, 1997) p. 91.

[3] K. Morita, K. Hiraga and Y. Sakka // *J. Am. Ceram. Soc.* **85** (2002) 1900.

[4] K. Morita, B.N. Kim, K. Hiraga and Y. Sakka // *Mat. Sci. Forum* **447-448** (2004) 329.

[5] K. Niihara // *J. Ceram. Soc. Japan* **99** (1991) 974.

[6] M.J. Mayo // *Nanostruct. Mater.* **9** (1997) 717.

[7] B.A.Cottom and M.J. Mayo // *Script Mater.* **34** (1996) 809.

[8] H. Kimura // *Advances in Powder Metallurgy & Particulate Mater-1999* (PM2TEC '99, Vancouver) **12** (1999) 55.

[9] G.D. Zhan, J. Kuntz, J. Wan and A.M. Mukherjee // *Nature Mater.* **2** (2003) 38.

[10] G.D. Zhan, J. Kuntz, J. Wan, J. Garay and A.M. Mukherjee // *J. Am. Ceram. Soc.* **86** (2003) 200.

[11] J.C. Wurst and J.A. Nelson // *J. Am. Ceram. Soc.* **55** (1972) 109.

[12] J.E. Bailey, D. Lewis, Z.M. Librant and L.J. Porter // *J. British. Ceram. Soc.* **71** (1972) 25.
[13] D.L. Hankey, R.A Graham, W.F. Hammetter and B. Morosin // *J. Mater. Sci. Lett.* **1**(1982) 445.
[14] K. Tsukuma, Y. Kubota and T. Tsukidate, In: *Advances in Ceramics,* Vol. 12 (Amrican Ceramic Society: Columbus, Ohio, 1984) p. 382.
[15] K. Tsukuma and K. Ueda // *J. Am. Ceram. Soc.* **68** (1985) C4.
[16] K. Tsukuma, K. Ueda, K. Matsushita and M. Shimada // *J. Am. Ceram. Soc.* **68** (1985) C56.
[17] M.V. Swain and L.R.F. Rose // *J. Am. Ceram. Soc.* **69** (1986) 511.
[18] A.G. Evans and R.M. Cannon // *Acta Mater.* **34** (1986) 761.
[19] P.M. Kelly and L.R.F. Rose // *Prog. Mater. Sci.* **47** (2002) 463.
[20] F.F. Lange // *J. Am. Ceram. Soc.* **66** (1983) 396.